J|A|C|S
ARTICLES
Published on Web 03/31/2007

Real-Time Observation of the Photoinduced Structural Change of Bis(2,9-dimethyl-1,10-phenanthroline)copper(I) by Femtosecond Fluorescence Spectroscopy: A Realistic Potential Curve of the Jahn−Teller Distortion

Munetaka Iwamura, Satoshi Takeuchi, and Tahei Tahara*

Contribution from the Molecular Spectroscopy Laboratory, RIKEN (The Institute of Physical and Chemical Research), 2-1 Hirosawa, Wako, Saitama 351-0198, Japan

Received December 26, 2006; E-mail: tahei@riken.jp

Abstract: In copper(I) complex $[Cu(dmphen)_2]^+$ (dmphen = 2,9-dimethyl-1,10-phenanthroline), a "flattening" structural change is induced with ^{1}MLCT excitation, which is a prototype of the structural change accompanied with Cu(I)/Cu(II) conversion in copper complexes. Femtosecond and picosecond emission dynamics of this complex were investigated in solution at room temperature with optically allowed $S_2 \leftarrow S_0$ photoexcitation. Time-resolved emission was measured in the whole visible region, and the lifetimes, intrinsic emission spectra, and radiative lifetimes of the transients were obtained by quantitative analysis. It was concluded that the initially populated S_2 state is relaxed with a time constant of 45 fs to generate the S_1 state retaining the perpendicular structure, and the $D_{2d} \rightarrow D_2$ structural change (the change of the dihedral angle between the two ligand planes) occurs in the S_1 state with a time constant of 660 fs. The intersystem crossing from the S_1 state to the T_1 state takes place after this structural distortion with a time constant of 7.4 ps. Importantly, the temporal spectral evolution relevant to the structural change clearly exhibited an isoemissive point around 675 nm. This manifests that there exists a shallow potential minimum at the perpendicular geometry on the S_1 surface, and the S_1 state stays undistorted for a finite period as long as 660 fs before the structural distortion. This situation is not expected for the structural change induced by the ordinary (pseudo-)Jahn−Teller effect, because the distortion should be induced by the spontaneous structural instability at the perpendicular structure. This result sheds new light on the present understanding on the structural change occurring in the metal complexes.

Introduction

Transition metal complexes usually show faster and more complicated excited-state dynamics than ordinary organic compounds because of their characteristic electronic properties, i.e., strong spin−orbit coupling and high density of states.[1] Elucidation of ultrafast electronic-state dynamics is very important for understanding this class of molecules, because it is responsible for a variety of fundamental phenomena including energy/electron transfers, magnetic properties, and structural changes in the excited state. However, it is very recently that ultrafast spectroscopy has been applied to the investigation of the ultrafast processes of metal complexes.[2−8] The electron/energy transfer, intersystem crossing, and electron localization process in porphyrins and ruthenium complexes have been studied so far. Nevertheless, little is known about the structural change in the excited state, although it often determines the photochemical properties of metal complexes.[9−11]

Copper(I) complex $[Cu(dmphen)_2]^+$ (dmphen = 2,9-dimethyl-1,10-phenanthroline) is a well-known prototypical metal complex that attracts much attention.[12−14] This complex exhibits strong absorption around 460 nm due to the metal-to-ligand charge transfer (MLCT) transition, and the photoexcitation gives rise to long-lived emission in the 700−800 nm region. Owing to these spectral properties, this complex is considered to be a promising candidate for the photocatalyst and photosensitizer in solar energy conversion and is claimed to have the potential to replace the well-known, but relatively expensive, metal complex $[Ru(bipyridine)_3]^{2+}$.[12−16] The most intriguing property of the $[Cu(dmphen)_2]^+$ complex is that it undergoes photoin-

(1) Vlček, A. J. *Coord. Chem. Rev.* **2000**, *200*−*202*, 933.
(2) Daniel, C. *Coord. Chem. Rev.* **2003**, *238*, 143.
(3) Forster, L. S. *Coord. Chem. Rev.* **2006**, *250*, 20023.
(4) Juban, E. A.; McCusker, J. K. *J. Am. Chem. Soc.* **2005**, *127*, 6857.
(5) Juban, E. A.; Smeigh, A. L.; Monat, J. E.; McCusker, J. K. *Coord. Chem. Rev.* **2006**, *250*, 1783.
(6) Damrauer, N. H.; Cerullo, G.; Yeh, A.; Boussie, T. R.; Shank, C. V.; McCusker, J. K. *Science* **1997**, *275*, 54.
(7) Yeh, A. T.; Shank, C. V.; McCusker, J. K. *Science* **2000**, *289*, 935.
(8) Bhasikuttan, A. C.; Suzuki, M.; Nakashima, S.; Okada, T. *J. Am. Chem. Soc.* **2002**, *124*, 8398.
(9) Kano, H.; Saito, T.; Kobayashi, T. *J. Phys. Chem. A* **2002**, *106*, 3445.
(10) Chen, L. X.; Jäger, W. J. H.; Jennings, G.; Gosztola, D. J.; Munkholm, A.; Hessler, J. P. *Science* **2001**, *292*, 262.
(11) Chen, L. X.; Shaw, G. B.; Novozhilova, I.; Liu, T.; Jennings, G.; Attenkofer, K.; Meyer, G. J.; Coppens, P. *J. Am. Chem. Soc.* **2003**, *125*, 7022.
(12) Kalyanasundaram, K. *Photochemistry of polypyridine and porphyrin complexes*; Academic Press: London, 1992.
(13) Scaltrito, D. V.; Thompson, D. W.; O'Callaghan, J. A.; Meyer, G. J. *Coord. Chem. Rev.* **2000**, *208*, 243.
(14) Roundhill, D. M. *Photochemistry and Photophysics of Metal Complexes*; Plenum Publishing Corporation: NewYork and London, 1994.
(15) Sakaki, S.; Kuroki, T.; Hamada, T. *J. Chem. Soc., Dalton Trans.* **2002**, 840.
(16) Armaroli, N. *Chem. Soc. Rev.* **2001**, *30*, 113.

10.1021/ja069300s CCC: $37.00

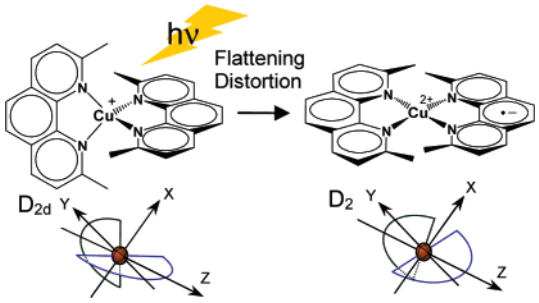

Figure 1. Photoinduced flattening distortion of $[Cu(dmphen)_2]^+$.

duced structural change.[11,13,14,17−26] With MLCT excitation, the central metal is formally oxidized from Cu(I) to Cu(II), and a structural change is induced as expected from the structural difference between Cu(I) complexes (tetrahedral-like) and Cu(II) complexes (square-planar-like) in the ground state. The dihedral angle between the two ligands becomes smaller with this "flattening" motion and the molecular symmetry of $[Cu(dmphen)_2]^+$ is reduced from D_{2d} to D_2, although the complex cannot reach the square planar structure because of the methyl groups at the 2 and 9 positions of the ligands (Figure 1). Such a structural change occurs not only with MLCT transition of $[Cu(dmphen)_2]^+$ but also in photochemical and electrochemical electronic conversion of Cu(I)/Cu(II) in general. Actually, it is suggested that this kind of structural distortion affects the electron-transfer rate of Cu complexes.[27−29] Furthermore, the structural change of the metal complexes has been attracting much interest in relation to numbers of applications such as molecular switches and artificial mastles.[29−33] Therefore, elucidation of the dynamics and mechanism of the structural change of copper complexes is very important not only for fundamental understanding but also for potential application of this series of metal complexes. In this sense, the $[Cu(dmphen)_2]^+$ complex provides a model system where we can directly investigate the dynamics of the structural distortion in real time, because the structural distortion is triggered by photoexcitation. It is noteworthy that a recent transient XAFS study by Chen et al. directly confirmed that the structure is certainly flattened in the ^{3}MLCT state of $[Cu(dmphen)_2]^+$.[11]

The driving force of the photoinduced structural change of $[Cu(dmphen)_2]^+$ is sometimes explained in terms of the Jahn−Teller effect.[11,13,17] In the crystal field theory, the energies of the d orbitals of the central copper are separated into four groups at the D_{2d} geometry, i.e., degenerated d_{xz} and d_{yz} and nondegenerated d_{xy}, $d_{x^2-y^2}$, and d_{z^2}, in the order of the energy. (The definition of the axis is shown in Figure 1.) With MLCT excitation, one electron is transferred from the Cu(I) (d^{10}) to the ligands and the electronic state of the resultant Cu(II) (d^9) is degenerated, and hence the structural change occurs to lower the molecular symmetry (the first-order Jahn−Teller effect). This simple explanation, however, is not relevant because the electronic state of the MLCT state is actually not degenerated when the molecular orbital of the whole molecule is considered. In fact, McMillin and co-workers pointed out that the photoinduced structural change of $[Cu(dmphen)_2]^+$ should be considered in terms of the pseudo Jahn−Teller effect (the second-order Jahn−Teller effect).[20] The Jahn−Teller distortion itself is one of the most fundamental issues in metal complexes and has been intensively studied from both experimental and theoretical sides.[34−37] However, the mechanism of photoinduced structural change of metal complexes has not been fully understood.

So far, several groups have applied time-resolved spectroscopy to the $[Cu(dmphen)_2]^+$ complex to clarify the excited-state dynamics, but their conclusions contradict each other.[11,17,38,39] Chen et al. carried out femtosecond transient absorption measurements and claimed that the structural change takes place in the time scale 10−20 ps. Nozaki and co-workers performed picosecond time-resolved fluorescence measurements and assigned the dynamics having a similar time constant (13 ps) to the intersystem crossing from the ^{1}MLCT to ^{3}MLCT state. This controversy implies that it is crucial to make unambiguous assignments of the transient species and distinguish the dynamics of the structural change from the other relaxation processes, in order to have a clear discussion about the photoinduced structural distortion of the $[Cu(dmphen)_2]^+$ complex.

In this paper, we report our femto- and picoseocnd time-resolved emission study of $[Cu(dmphen)_2]^+$ in dichloromethane.[40] Time-resolved emission spectroscopy is advantageous over time-resolved absorption spectroscopy, because it monitors the optical transition between the excited state in question and the ground state so that it can provide not only the lifetime but also other important quantities including radiative lifetimes, emission spectra, and energy levels of the transients. These quantities are crucial for assignment of the transients and dynamics observed. We measured time-resolved emission signals in a wide wavelength region over the whole visible region and made unambiguous assignments of the observed excited-state dynamics, including the ultrafast structural distortion. The present study clearly indicates that a short-lived precursor state appears in the S_1 potential before the structural distortion. This is not expected for the structural change induced by the ordinary (pseudo-) Jahn−Teller effect and, hence, requests the revision

(17) Siddique, Z. A.; Yamamoto, Y.; Ohno, T.; Nozaki, K. *Inorg. Chem.* **2003**, *42*, 6366.
(18) Zgierski, M. Z. *J. Chem. Phys.* **2003**, *118*, 4045.
(19) Shinozaki, K.; Kaizu, Y. *Bull. Chem. Soc. Jpn.* **1994**, *67*, 2435.
(20) Cunningham, C. T.; Moore, J. J.; Cunningham, K. L. H.; Fanwick, P. E.; McMillin, D. R. *Inorg. Chem.* **2000**, *39*, 3638.
(21) Cody, J.; Dennisson, J.; Gilmore, J.; VanDerveer, D. G.; Henary, M. M.; Gabrielli, A.; Sherrill, C. D.; Zhang, Y.; Pan, C.-P.; Burda, C.; Fahrni, C. J. *Inorg. Chem.* **2003**, *42*, 4918.
(22) Kovalevsky, A. Y.; Gembicky, M.; Novozhilove, I. V.; Coppens, P. *Inorg. Chem.* **2003**, *42*, 8794.
(23) Kovalevsky, A. Y.; Gembicky, M.; Coppens, P. *Inorg. Chem.* **2004**, *43*, 8282.
(24) Sakaki, S.; Mizutani, H.; Kase, Y. *Inorg. Chem.* **1992**, *31*, 4575.
(25) Waterland, M. R.; Howell, S. L.; Gordon, K. C.; Burrell, A. K. *J. Phys. Chem. A* **2005**, *109*, 8826.
(26) Kalsani, V.; Schmittel, M. *Inorg. Chem.* **2006**, *45*, 2061.
(27) Koshino, N.; Kuchiyama, Y.; Ozaki, H.; Funabashi, S.; Takagi, H. D. *Inorg. Chem.* **1999**, *38*, 3352.
(28) Sykes, A. G. *Struct. Bonding* **1991**, *75*, 175.
(29) Rorabacher, D. B. *Chem. Rev.* **2004**, *104*, 651.
(30) Wang, Y.; Teng, F.; Xu, Z.; Qian, L.; Zhang, T.; Liu, D. *Prog. Nat. Sci.* **2004**, *14*, 745.
(31) Nishihara, H. *Bull. Chem. Soc. Jpn.* **2004**, *77*, 407.
(32) Balzani, V.; Credi, A.; Raymo, F., M.; Stoddart, J. F. *Angew. Chem., Int. Ed.* **2000**, *39*, 3348.
(33) Sato, O. *Acc. Chem. Res.* **2003**, *36*, 692.
(34) Jahn, H. A.; Teller, E. *Proc. R. Soc. London* **1937**, *161A*, 220.
(35) Person, R. G. *Proc. Nat. Acad. Sci. U.S.A.* **1975**, *72*, 2104.
(36) Person, R. G. *J. Mol. Struct.* **1983**, *103*, 25.
(37) Bersuker, I. B. *The Jahn-Teller Effect*; Cambridge University Press: Cambridge, 2006.
(38) Gunaratne, T.; Rodgers, M. A. J.; Felder, D.; Nierngarten, J.-F.; Accorsi, G.; Armaroli, N. *Chem. Commun.* **2003**, 3010.
(39) Samia, A. C. S.; Cody, J.; Fahrni, C. J.; Burda, C. *J. Phys. Chem. B* **2004**, *108*, 563.
(40) Tahara, T. *Advances in Multiphoton Processes and Spectroscopy*; World Scientific, 2004; Vol. 16, p 1.

of the present understanding of the photoinduced structural change that occurs in the MLCT state of the metal complexes.

Experimental Section

Sample. $[Cu(dmphen)_2]PF_6$ was prepared by the method reported in the literature.[41] The purity of the sample was checked by the elemental analysis and absorption. Dichloromethane (Wako, HPLC grade), acetonitrile (Wako, HPLC grade), and butyronitrile (Wako, first grade) were used without further purification. We prepared a fresh sample solution for each time-resolved measurement. The concentrations of the samples are 0.01 mol dm^{-3} for the dichloromethane solution and 0.005 mol dm^{-3} for the acetonitrile and butyronitrile solutions. The stability of the sample was checked by comparing absorption spectra before and after the measurements.

Measurements. Steady-state absorption and emission spectra were recorded by commercial spectrometers (U-3310, Hitachi and FluoroLog 3, Spex).

Picosecond time-resolved emission measurements were carried out using a streak camera system (C4334, Hamamatsu). To generate excitation pulses at 550 nm or 420 nm, we used a Ti:sapphire regenerative amplifier (Spitfire, Spectra-Physics) seeded by a Ti:sapphire femtosecond mode-locked laser (Tsunami, Spectra-Physics). The amplified pulse was converted to a near-infrared pulse (1760 nm) in an optical parametric amplifier (TOPAS, Quantronix), and it was sum-frequency-mixed with the fundamental pulse (800 nm) to generate the 550-nm pulse. To obtain excitation pulses at 420 nm, the output of the optical parametric amplifier (1680 nm) was frequency-quadrupled by using two β-BaB_2O_4 crystals. The sample solution was contained in a cell with a thickness of 1 mm, and the emission was collected through a polarizer with the backscattering geometry. The polarization of the excitation and detection was set at the magic angle. Time-resolved traces were measured in sweep ranges of 1 and 100 ns with instrumental response times (fwhm) of 20 ps and 1 ns, respectively. All measurements were performed at room temperature (299 K).

Quinine in 1 N H_2SO_4 aqueous solution and 4-dimethylamino-4′-nitrostilbene in *o*-dichlorobenzene were used references for correction of the wavelength-dependent instrumental sensitivity in the steady-state and time-resolved emission measurements.[42]

The experimental setup for the femtosecond fluorescence up-conversion measurement is essentially the same as that described previously.[43] The light source was a mode-locked Ti:sapphire laser (Coherent, MIRA) that produced a 1400-mW pulse train at 840 nm with a typical pulse duration of 105 fs. This fundamental pulse was converted to the second harmonic pulse at 420 nm by using a β-BaB_2O_4 crystal (0.2 mm thickness). The generated second harmonic pulse was focused into a thin-film-like jet stream of the sample solution for photoexcitation. The residual fundamental pulse after the second harmonic generation was used as a gate pulse for the up-conversion process. The fluorescence from the sample was collected and focused into a β-BaB_2O_4 mixing crystal with use of an aluminum-coated elliptic mirror. A cutoff filter was placed between the mirror and the mixing crystal to block the excitation light. The fluorescence was up-converted by type-I sum-frequency generation with the gate pulse in the mixing crystal. The up-converted signal was separated from other lights by an iris, band-pass filters, and a monochromator (HR-320, Jobin Yvon), and then it was detected by a photon-counting photomultiplier with a counter (SR-400, Stanford Research Systems). The fluorescence was detected at the magic angle by rotating the excitation polarization with respect to the gate polarization. The time resolution was evaluated as ~200 fs by the up-conversion measurement for the Raman signal from the solvent.

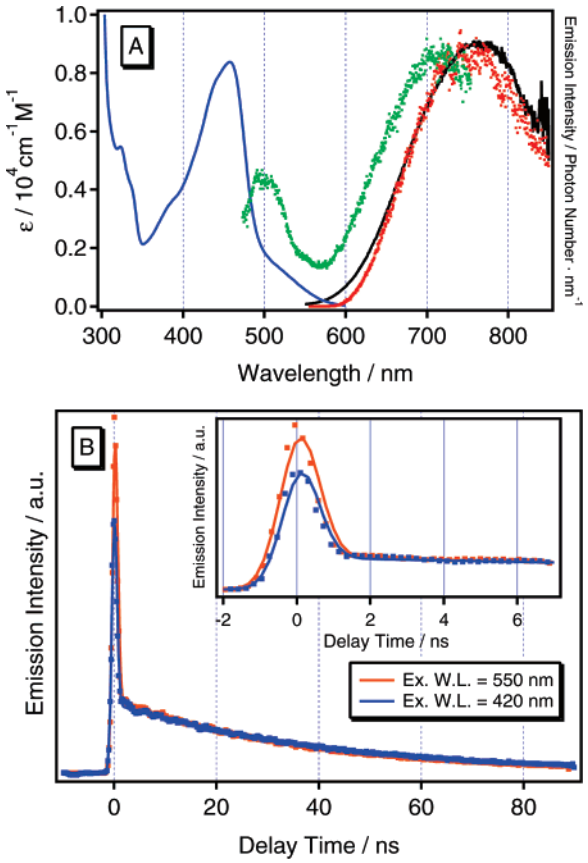

Figure 2. (A) Absorption, steady-state, and time-resolved emission spectra of $[Cu(dmphen)_2]^+$ in dichloromethane at room temperature. Blue line: absorption spectrum. Black line: the steady-state emission spectrum. Green dots: the time-resolved emission spectrum in the −0.05 to 0.05 ns region after removing a Roman signal of the solvent. Red dots: the time-resolved emission spectrum in the 2−100 ns region. Excitation wavelength was 420 nm, and the sample concentration was 1×10^{-2} mol dm^{-3}. (B) Time-resolved emission signals of $[Cu(dmphen)_2]^+$ in dichloromethane observed with excitation wavelength at 420 nm (S_2 excitation; blue) and 550 nm (S_1 excitation; orange). These traces were obtained by the signal integration of the data measured by a streak camera in the wavelength region from 650 to 800 nm. The sample concentration was 1×10^{-2} mol dm^{-3}.

Results and Discussion

Emission Dynamics Observed in Picosecond Measurements. Figure 2A depicts the absorption and emission spectra of $[Cu(dmphen)_2]^+$ in dichloromethane. The molecule shows absorption bands in the visible region due to the ^{1}MLCT transitions (the blue curve). A strong band around 460 nm is assigned to the $S_2 \leftarrow S_0$ transition, whereas a weak band around 550 nm is attributed to the $S_1 \leftarrow S_0$ transition which is recognized as a tail of the 460 nm band.[17,18,44] With the S_2 excitation (420 nm), the $[Cu(dmphen)_2]^+$ complex exhibits steady-state emission in the 700−800 nm region (the black curve). This broad emission has been assigned to the phosphorescence from the ^{3}MLCT state, which is generated by the intersystem crossing from the ^{1}MLCT state. (Although this emission has a contribution of the delayed fluorescence,[45] we call it just phosphorescence in this paper for simplicity.)

We first examined the emission dynamics of $[Cu(dmphen)_2]^+$ in the pico- and nanosecond time region using a streak camera

(41) McMillin, D. R.; Buckner, M. T.; Tae Ahn, B. *Inorg. Chem.* **1976**, *16*, 943.
(42) Lippert, E.; Nagele, W.; Seibold-Blankenstein, I.; Staiger, W.; Voss, W. *Z. Anal. Chem.* **1959**, *170*.
(43) Takeuchi, S.; Tahara, T. *J. Phys. Chem. A* **1997**, *101*, 3052.
(44) Parker, W. L.; Crosby, G. A. *J. Phys. Chem.* **1989**, *93*, 5692.
(45) Kirchhoff, J. R.; Gamache, R. E. J.; Blaskie, M. W.; Delpaggio, A. A.; Lengel, R. K.; McMillin, D. R. *Inorg. Chem.* **1983**, *22*, 2380.

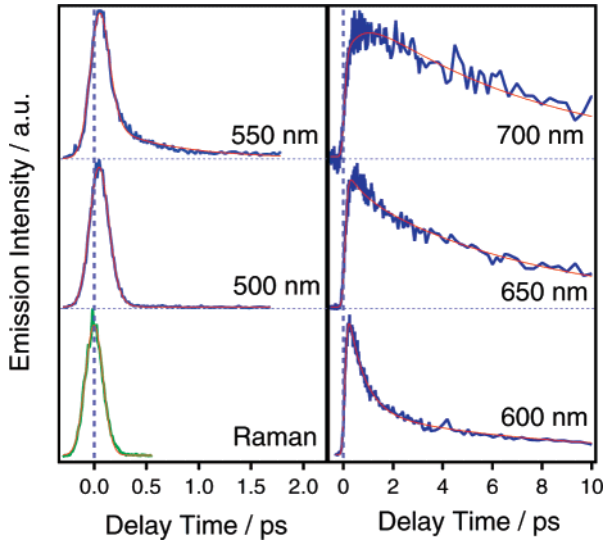

Figure 3. Time-resolved emission signals of $[Cu(dmphen)_2]^+$ in dichloromethane measured at various wavelengths by the up-conversion method (420 nm excitation; 1×10^{-2} mol dm^{-3}). The temporal profile Raman scattering of dichloromethane is also given to show the instrumental response function.

with S_2 excitation (420 nm). Figure 2B shows a time-resolved emission trace obtained by signal integration over the 650−800 nm region (blue line). The initial spikelike component could not be time-resolved in the streak camera measurement, but the second slow component clearly exhibited a single-exponential decay with a time constant of 41 ns. The phosphorescence lifetime of this metal complex has been reported to be 90 ns (degassed condition) and 55 ns (air saturated condition),[45] which agree well with the lifetime observed. Therefore, the slow component was attributed to the phosphorescence from the ^{3}MLCT state. In fact, the emission spectrum of the slow component (integration over the 2−100 ns region; the red curve in Figure 2A) accords with the steady-state spectrum, which assures this assignment. Chen et al. showed that the structure of the ^{3}MLCT state that appears in the nanosecond time region is already distorted from the perpendicular geometry by the transient XAFS spectroscopy.[11] Thus, the slow emission is attributed to the phosphorescence from the ^{3}MLCT state after the structural distortion. The emission spectrum corresponding to the spikelike feature (integration over the −0.05 to 0.05 ns time region; the green curve in Figure 2A) shows two characteristic peaks around 500 and 720 nm, and it is quite different from the steady-state emission spectrum. This indicates that the ultrafast emission dynamics exists in the femtosecond and/or early picosecond time region, including the dynamics relevant to the structural distortion.

Emission Dynamics Observed in Femtosecond Measurements. Femtosecond time-resolved emission signals of $[Cu(dmphen)_2]^+$ in dichloromethane were measured in the wavelength region 475−725 nm by the up-conversion method with the same 420-nm excitation. As shown in Figure 3, the temporal behavior of the signals varies significantly depending on the observation wavelength. In the short wavelength region (500 nm), there appears an ultrafast component that decays with a time constant as short as $\tau_1 = 45$ fs. As the observation wavelength becomes longer (600 nm), the signal shows a slower decay with a time constant of $\tau_2 = 660$ fs. In the longest wavelength region (700 nm), the signal shows a rising feature,

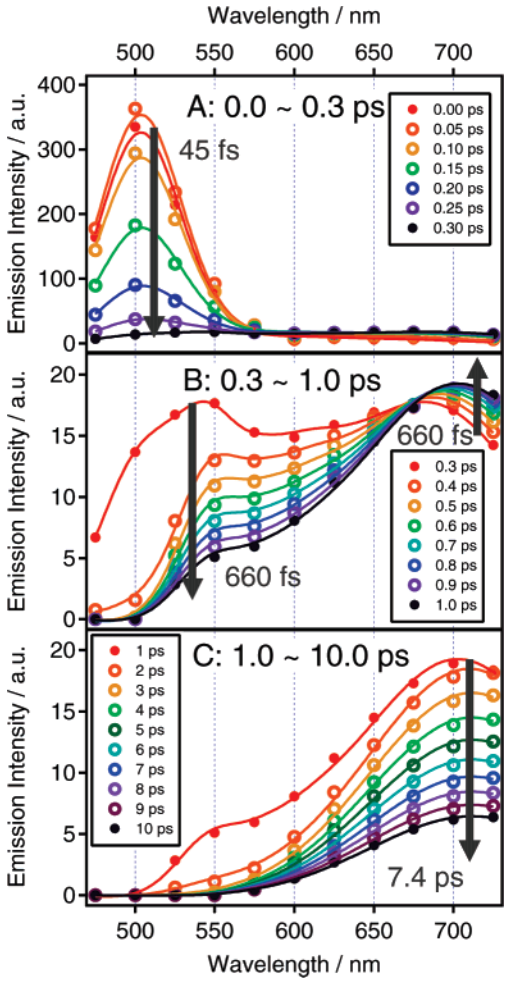

Figure 4. Time-resolved emission spectra of $[Cu(dmphen)_2]^+$ in dichloromethane in the time region 0.0−0.3 ps (A), 0.3−1.0 ps (B), and 1.0−10.0 ps (C) (420 nm excitation; 1×10^{-2} mol dm^{-3}).

which is followed by a much slower decaying component having a time constant of $\tau_3 = 7.4$ ps. The phosphorescence emission from the ^{3}MLCT state (41 ns lifetime) was not recognized in this up-conversion measurement because of its very weak time-resolved intensity, although it is dominant in the (time-integrated) steady-state emission spectrum.

To reconstruct time-resolved emission spectra from the time-resolved traces observed, we corrected the wavelength-dependent up-conversion efficiency in the following way. We used a picosecond time-resolved emission spectrum as a reference, which was obtained by integration of the streak camera data over the −0.05−0.05 ns time region (the green curve in Figure 2A). This reference spectrum does not contain the ^{3}MLCT phosphorescence in a practical sense but includes only the short-lived emission components that contribute to the up-conversion signal. We normalized the intensity of the up-conversion signal so that its relevant time-integrated value is proportional to the reference intensity at each wavelength. The reconstructed time-resolved emission spectra are shown in Figure 4. These spectra clearly exhibit characteristic spectral change, corresponding to the three decay components. These three components are obviously ascribed to the emissions from singlet states because the phosphorescence is much weaker. Immediately after photoexcitation, a very strong emission band appears around 500 nm and decays rapidly, which corresponds to the 45-fs decay

component (Figure 4A). This 500-nm band corresponds to the emission peak around 500 nm in the picosecond time-resolved spectrum shown in Figure 2. Because this band appears simultaneously with photoexcitation and exhibits a mirror image of the S_2 absorption band, it is assignable to the fluorescence from the initially populated S_2 state. As the S_2 fluorescence decays, the time-resolved emission exhibits a broad spectrum extending from 550 to 750 nm, which is in the longer wavelength region than the S_1 absorption. This fluorescence appears in accordance with the decay of the S_2 state, so that it is naturally attributed to the fluorescence from the S_1 state that is generated by the internal conversion from the S_2 state. In the following subpicosecond region, the short-wavelength side of the broad spectrum becomes weak, whereas the long-wavelength side rises, with a common time constant of $\tau_2 = 660$ fs. This spectral evolution shows a clear isoemissive point at 675 nm, indicating that it is ascribed to the conversion from one emissive transient to another. This spectral change finally results in the third emission band around 725 nm, which decays with the time constant $\tau_3 = 7.4$ ps. The spectrum and the lifetime of this 7.4-ps emission agree well with those of the emission observed in a previous picosecond fluorescence study by Nozaki and co-workers, who assigned it to the fluorescence from the S_1 state *after* the structural distortion.[17] The excited molecule should hold the initial perpendicular conformation immediately after photoexcitation, and therefore, the spectral evolution occurring with a time constant of 660 fs is attributable to the structural distortion from the perpendicular form (S_1^{perp}) to the "flattened" form ($S_1^{flattened}$) taking place in the S_1 state. (The experiments on the solvent viscosity dependence was fully consistent with this assignment. *Vide infra.*) The emission spectrum of the $S_1^{flattened}$ state corresponds to the 720-nm band in the picosecond time-resolved spectrum in the early delay time. The spectrum of the $S_1^{flattened}$ state is slightly but significantly blue-shifted compared with the phosphorescence spectrum observed in the later delay time. Because the spectral evolution from the $S_1^{flattened}$ fluorescence ($\lambda_{max} = 720$ nm) to the phosphorescence ($\lambda_{max} = 750$ nm) has been observed in the streak camera measurement, it can be concluded that the $S_1^{flattened}$ state is relaxed to the ^{3}-MLCT state ($T_1^{flattened}$) by intersystem crossing.

The reconstructed femtosecond time-resolved emission spectra, in combination with the picosecond data, directly showed that the following emissive excited states appear in the cascaded relaxation process after S_2 excitation of $[Cu(dmphen)_2]^+$:

$$S_0^{perp} \xrightarrow{h\nu} S_2^{perp} \xrightarrow{IC} S_1^{perp} \xrightarrow{\text{structural distortion}} S_1^{flattened} \xrightarrow{ISC} T_1^{flattened} \rightarrow$$

Quantitative Analysis and Emission Spectra of Each Transient. The time-resolved emission data showed that the three emissive excited singlet states (S_2^{perp}, S_1^{perp}, $S_1^{flattened}$) participate in the relaxation process of $[Cu(dmphen)_2]^+$, in addition to the long-lived $T_1^{flattened}$. This assignment was firmly confirmed by the quantitative analysis of the fluorescence up-conversion data described below, which provided radiative rate constants (oscillator strengths) of transient species.[40,43,46,47]

We carried out the analysis of the femtosecond fluorescence data based on the following relaxation scheme,

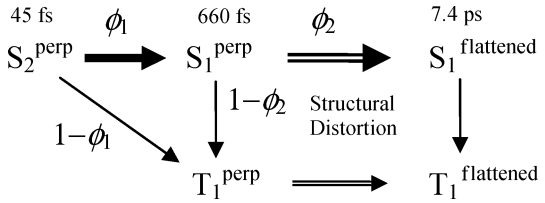

where ϕ_1 and ϕ_2 denote the quantum yield of the $S_2^{perp} \rightarrow S_1^{perp}$ internal conversion and that of the $S_1^{perp} \rightarrow S_1^{flattened}$ structural relaxation, respectively. This scheme includes the initially populated S_2^{perp} state, the lowest excited singlet and triplet states before (S_1^{perp}, T_1^{perp}) and after ($S_1^{flattened}$, $T_1^{flattened}$) the structural change. We included the T_1^{perp} state in the scheme although this transient was not directly observed in the time-resolved emission measurements. It is because the intersystem crossing of metal complexes often takes place in the subpicosecond time scale, and hence it could be a competing process for the internal conversion and structural distortion.[6,8] Solving a set of rate equations with an initial condition that only the photoexcited S_2^{perp} state is populated at $t = 0$, we obtained analytical expressions for the time-dependent population ($[S_2^{perp}(t)]$, etc.) of each state (see Supporting Information for details). Because the observed up-conversion signal is the sum of the contribution from the three excited singlet states (S_2^{perp}, S_1^{perp}, and $S_1^{flattened}$), it can be written as,

$$I(t,\lambda) = a_1(\lambda)[S_2^{perp}(t)] + a_2(\lambda)[S_1^{perp}(t)] + a_3(\lambda)[S_1^{flattened}(t)] \quad (1a)$$

$$= A_1 \exp(-k_1 t) + A_2 \exp(-k_2 t) + A_3 \exp(-k_3 t) \quad (1b)$$

where $a_i(\lambda)$ represents the intrinsic fluorescence transition probability of each excited state. The $a_i(\lambda)$'s are related to the amplitudes of exponential components (A_i's) that are directly determined by the fitting analysis of the data,

$$a_1(\lambda) = A_1 + A_2 + A_3 \quad (2a)$$

$$a_2(\lambda) = \frac{1}{\phi_1 \cdot k_1}[(k_1 - k_2)A_2 + (k_1 - k_3)A_3] \quad (2b)$$

$$a_3(\lambda) = \frac{1}{\phi_1 \cdot \phi_2 \cdot k_1 \cdot k_2}[(k_1 - k_3)(k_2 - k_3)A_3] \quad (2c)$$

where $k_i = 1/\tau_i$ is the decay rate constants that were already determined experimentally. We determined the A_i values at every wavelength by the fitting analysis of the up-conversion data. The values of a_1, $\phi_1 \cdot a_2$, and $\phi_1 \cdot \phi_2 \cdot a_3$, which are obtained by eqs 2a−c, are plotted against the wavelength in Figure 5. The a_i spectrum represents the intrinsic emission spectrum of each excited state. The integration of the a_i spectrum (in the frequency domain) gives the number of emitted photons within the unit time,[48] so that it is proportional to the radiative rate constant (k_{ri}). From the integration of the three spectra in Figure 5, we obtained the ratio for the radiative rate constants of S_2^{perp}, S_1^{perp}, and $S_1^{flattened}$ states as $k_{r1}:(\phi_1 \cdot k_{r2}):(\phi_1 \cdot \phi_2 \cdot k_{r3}) = 32:1.2:1.0$. Note that the ϕ factors appear here, because the relaxation path to T_1^{perp} is taken into account in the scheme.

(46) Takeuchi, S.; Tahara, T. *Chem. Phys. Lett.* **1997**, *277*, 340.
(47) Takeuchi, S.; Tahara, T. *J. Phys. Chem. A* **1998**, *102*, 7740.

(48) In this study, the calibration was performed so that the intensities of the spectra were represented in the unit of photon number/nm. Therefore, a_i was also given in the unit of photon number/nm.

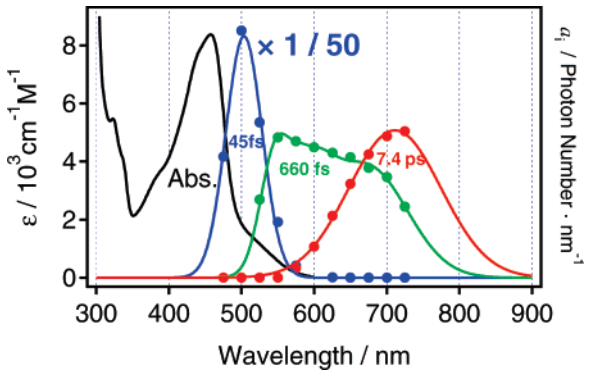

Figure 5. Fluorescence spectra of the three components observed in the up-conversion experiments of $[Cu(dmphen)_2]^+$ in dichloromethane. Blue curve: the 45-fs component (a_1). Green curve: the 660-fs component ($\phi_1 \cdot a_2$). Red curve: the 7.4 ps component ($\phi_1 \cdot \phi_2 \cdot a_3$). The absorption spectrum is also shown for comparison. Solid curves represent the fits to the fluorescence spectra using single or multipeak Gaussian line shape functions.

Absolute Radiative Rate Constants. The absolute radiative rate constants can be obtained from the above ratio, by relating the ratio to the apparent radiative rate constant of phosphorescence at room temperature which was evaluated as 2.3×10^3 s^{-1}.[45,49] We determined the intensity ratio between the phosphorescence and the other fluorescence components from the time-resolved emission data taken by the streak camera with S_2 photoexcitation (Figure 2B, blue line), where the emissions from the S_1^{perp}, $S_1^{flattened}$, and $T_1^{flattened}$ states contribute to the signal. (Note that the S_2^{perp} fluorescence is out of the detection wavelength region and the T_1^{perp} emission should be negligibly weak because of its short lifetime and small radiative rate constant.) The long-lived component seen in the nanosecond region is due to the phosphorescence, whereas the spikelike feature around the time origin arises from the S_1^{perp} and $S_1^{flattened}$ fluorescence. We represented the temporal behavior of the emission as $I(t) = c(a_2[S_1^{perp}(t)] + a_3[S_1^{flattened}(t)] + a_4[T_1^{flattened}(t)])$, where the coefficients a_2 and a_3 were obtained by integrating the $a_2(\lambda)$ and $a_3(\lambda)$ in the 650−800 nm region and a_4 is the phosphorescence transition probability. The lifetimes of the three transients were fixed at $\tau_2 = 660$ fs, $\tau_3 = 7.4$ ps, and $\tau_4 = 41$ ns. We convoluted this function with the instrumental response of the streak camera measurement and fitted it to the time-resolved data in Figure 2B to evaluate the parameters a_4 and c. From this analysis, the relative radiative rate constants of the S_1^{perp}, $S_1^{flattened}$, and $T_1^{flattened}$ states were determined as $(\phi_1 \cdot k_{r2}):(\phi_1 \cdot \phi_2 \cdot k_{r3}):(k_{r4}) = 1.2:1.0:0.0021$.[50] (See Supporting Information for details of the procedure to obtain the absolute oscillator strengths using phosphorescence intensity as a reference.) Since we know the absolute value of the apparent radiative decay rate of phosphorescence at room temperature ($k_{r4} = 2.3 \times 10^3$ s^{-1}), the radiative rate constants (with the ϕ factors) of the other excited singlet states were evaluated as $k_{r1} = 3.6 \times 10^7$ s^{-1}, $\phi_1 \cdot k_{r2} = 1.3 \times 10^6$ s^{-1}, and $\phi_1 \cdot \phi_2 \cdot k_{r3} = 1.1 \times 10^6$ s^{-1}.

The evaluated radiative rate constant of the S_2^{perp} state (k_{r1}) is in very good agreement with the value obtained by the integration of the S_2 band in the absorption spectrum (3.6×10^7 s^{-1}), which assures the assignment. Concerning the $S_1^{flattened}$ and S_1^{perp} states, we need to evaluate the relaxation quantum yields, ϕ_1 and ϕ_2, to obtain the absolute radiative rate constants.

The ϕ_1 value, the quantum yield of the $S_2^{perp} \rightarrow S_1^{perp}$ internal conversion, can be directly evaluated by the comparison of time-resolved emission data obtained with the S_1^{perp} and S_2^{perp} excitation. The nanosecond emission signals obtained with the S_2^{perp} (420 nm, blue curve) and S_1^{perp} (550 nm, red curve) excitations are compared in Figure 2B, in which the intensity is normalized for the long-lived phosphorescence intensity due to $T_1^{flattened}$. Clearly, the amplitude of the spikelike feature due to the S_1^{perp} and $S_1^{flattened}$ emissions becomes smaller when the complex is initially photoexcited to the S_2^{perp} state. (Note that the signals do not contain any S_2^{perp} fluorescence because they were obtained by the signal integration in the 650−800 nm region.) It means that, in the case of S_2 excitation, a significant portion of $T_1^{flattened}$ is generated not from the $S_1^{perp} \rightarrow S_1^{flattened} \rightarrow T_1^{flattened}$ pathway but through the $T_1^{perp} \rightarrow T_1^{flattened}$ pathway that is "dark" in the emission spectroscopy. In other words, the $S_2^{perp} \rightarrow T_1^{perp}$ intersystem crossing process is not negligible, i.e., $\phi_1 < 1$. To evaluate ϕ_1 values, we used analytical expressions for the temporal behavior of the emission intensity, $I(t,\lambda) = a_1(\lambda)[S_2^{perp}(t)] + a_2(\lambda)[S_1^{perp}(t)] + a_{2'}(\lambda)[T_1^{perp}(t)] + a_3(\lambda)[S_1^{flattened}(t)] + a_4(\lambda)[T_1^{flattened}(t)] = A_1 \exp(-k_1 t) + A_2 \exp(-k_2 t) + A_{2'} \exp(-k_{2'} t) + A_3 \exp(-k_3 t) + A_4 \exp(-k_4 t)$, as well as the relation between the coefficients a_i and the amplitudes A_i ($1/k_{2'}$ is the lifetime of T_1^{perp}). With reasonable approximations ($a_1, a_2, a_3 \gg a_4, a_{2'}$; $k_1 \gg k_2, k_{2'} \gg k_3 \gg k_4$), we obtained the following simple expression that relates the ϕ_1 value to the amplitude ratio of A_i's that are obtained with the S_2^{perp} and S_1^{perp} excitation (see Supporting Information for details):

$$\phi_1 = (A_3/A_4)_{S2exc}/(A_3/A_4)_{S1exc} = (A_2/A_4)_{S2exc}/(A_2/A_4)_{S1exc} \quad (4)$$

Practically, it means that the ϕ_1 value can be determined from the relative intensity of the spikelike feature observed with S_2^{perp} and S_1^{perp} excitation. We determined the A_i values by the fitting analysis of the nanosecond time-resolved traces shown in Figure 2B and evaluated the ϕ_1 value as $\phi_1 = 0.7$.

The ϕ_2 value, the quantum yield of the $S_1^{perp} \rightarrow S_1^{flattened}$ structural relaxation, could not be determined directly from the experimental data. Nevertheless, we considered this value close to unity ($\phi_2 \approx 1$) because the lifetime of the S_1^{perp} state significantly changed with the change of the solvent viscosity. Figure 6 shows femtosecond time-resolved emission signals of $[Cu(dmphen)_2]^+$ measured in two solvents having different viscosities, acetonitrile ($\eta = 0.36$ mPas) and butyronitrile ($\eta = 0.59$ mPas).[51] As shown in Figure 6A, a remarkable difference was observed for the decay of the emission at 600 nm, to which the fluorescence from the S_1^{perp} state mainly contributes. The fitting analysis showed that the lifetime of the S_1^{perp} state changed from 340 fs (acetonitrile) to 500 fs (butyronitrile) as the solvent viscosity was increased. This large solvent dependence indicated that the lifetime of the S_1^{perp} state is predominantly determined by a relaxation process whose rate is largely

(49) The apparent radiative rate constant of phosphorescence depends on the temperature because of the change of the relative contribution from delayed fluorescence. We obtained the value of 2.3×10^3 s^{-1} using the emission yield (ϕ_{em}) and lifetime (τ) at room temperature, which were reported in ref 45, with the equation $\phi_{em}/\tau = k_r$.

(50) Here, the whole emission yields were evaluated from the data in the wavelength region 650−800 nm. Ratios of the area intensity in the 650−800 nm region to that of whole region were evaluated as 0 % for a_1, 37 % for a_2, 75 % for a_3, and 65 % for a_4. See Figure S2 in the Supporting Information.

(51) Adam, W.; Diedering, M.; Trofimov, A. V. *Phys. Chem. Chem. Phys.* **2002**, *4*, 1036.

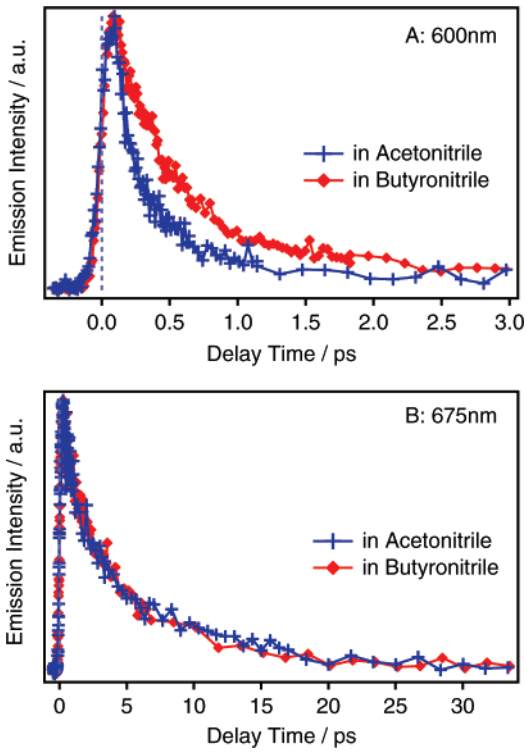

Figure 6. Time-resolved emission signals of $[Cu(dmphen)_2]^+$ in acetonitrile (blue line) and butyronitrile (red line) at 600 nm (A) and 675 nm (B) (420 nm excitation; 5×10^{-3} mol dm^{-3}).

affected by the solvent viscosity. Thus, the major relaxation pathway of the S_1^{perp} state is not the intersystem crossing but the structural change. We note that the change of the solvent did not induce any noticeable influence on the emission dynamics at 675 nm in the early picosecond time region (Figure 6B), which manifests that the dynamics of the $S_1^{flattened} \rightarrow T_1^{flattened}$ intersystem crossing is not affected by the solvent viscosity. These data on the viscosity dependence indicates that the intersystem crossing of the S_1^{perp} state is slow compared with its structural change. This seems reasonable because the intersystem crossing of the $S_1^{flattened}$ is also slow ($1/7.4 \times 10^{12}$ s^{-1}). In fact, if we assume the intersystem crossing rate of the S_1^{perp} state to be the same as that of the $S_1^{flattened}$ state, the ϕ_2 value is calculated as 0.92. It may be also noteworthy that the apparent radiative rate constants of the S_1^{perp} ($\phi_1 \cdot k_{r2}$) and S_1^{Flat} ($\phi_1 \cdot \phi_2 \cdot k_{r3}$) states are very similar. Because it is unlikely that the radiative rate of the $S_1^{flattened}$ state (k_{r3}) is much larger than that of the S_1^{perp} state (k_{r2}), this also suggests that the ϕ_2 value is close to unity.[52]

We need to discuss the previous estimation by Nozaki and co-workers, who estimated the yield of the $S_1^{flattened}$ state as 0.1 in the case of S_2 excitation.[17] (This value corresponds to $\phi_1 \times \phi_2 = 0.7$ in our estimation.) Their value was estimated from a comparison between the radiative rate constant determined by time-resolved fluorescence measurements ($k_r = 2.2 \times 10^6$ s^{-1}) and that obtained from the Arrhenius plot for the delayed fluorescence intensity reported by Kirchhoff et al. ($k_r = 2 \times 10^7$ s^{-1}).[45] Their estimation is correct in principle, but it contains a very large error. As for the k_r value evaluated from the Arrhenius plots for example, we note that this value heavily depends on the estimation of the energy difference between $S_1^{flattened}$ and $T_1^{flattened}$ (ΔE). Actually, the error of ΔE was reported as 20% ($\Delta E = (1.8 \pm 0.4) \times 10^3$ cm^{-1}) in the original paper of Kirchhoff et al.,[45] which gives a k_r value from 1.5×10^8 s^{-1} to 3.2×10^6 s^{-1}. The quantum yield of the $S_1^{flattened}$ state that is calculated from this range of the k_r values are 0.01−0.6. Considering other possible experimental errors, e.g., the error in the estimations of emission yields and lifetimes, our value (0.7) can be within the range of their error. Therefore, it is reasonable to consider that the ϕ_2 value is close to unity at the moment, although the arguments given above are more or less semiquantitative. Hereafter, we regard the ϕ_2 value as unity, keeping it in our mind that it may contain a relatively large error.

Using the quantum yields of $\phi_1 = 0.7$ and $\phi_2 = 1$, we can finally obtain all the absolute radiative rate constants of the S_2^{perp}, S_1^{perp}, and $S_1^{flattened}$ states as $k_{r1} = 3.6 \times 10^7$ s^{-1}, $k_{r2} = 1.8 \times 10^6$ s^{-1}, and $k_{r3} = 1.6 \times 10^6$ s^{-1}. These values are summarized in Table 1, along with other photochemical quantities of all the excited states observed.

On the basis of the transient absorption data, Chen et al. argued that the intersystem crossing takes place with a time constant of 500−700 fs and then the structural change occurs with a time constant of 10−20 ps in the T_1 state.[11] The present study clearly denies their arguments. The transient that appears with a time constant of 660 fs from the S_1^{perp} state (which was assigned to the $S_1^{flattened}$ state in this study) has a large radiative rate constant comparable to that of the S_1^{perp} state. It means that the relaxation of the S_1^{perp} state proceeds on the S_1 potential surface. In addition, the lifetime of the S_1^{perp} state is significantly affected by the solvent viscosity, which is fully consistent with that the relaxation is the structural change. Furthermore, the relaxation process proceeding with a time constant of 7.4 ps (which was assigned to $S_1^{flattened} \rightarrow T_1^{flattened}$) is accompanied with the generation of the transient that has a much smaller radiative rate constant. Thus, this process is definitely attributed to the intersystem crossing. In this sense, the present study agrees with the argument of Nozaki and co-workers who claimed that the intersystem crossing of $[Cu(dmphen)_2]^+$ takes place in a time scale as long as 10 ps.[17] It is noteworthy that the time constants of the intersystem crossing of the metal complexes are often considered to be shorter than a picosecond in general, because of the very short intersystem crossing time reported for several well-known metal complexes. For example, it was reported as 40 fs for $[Ru(bipyridine)_3]^{2+}$ and less than 1 ps for some typical Cr(III) complexes.[1,3−5,8] In this sense, the intersystem crossing of the S_1 state of $[Cu(dmphen)_2]^+$ is slow. However, it might be too early to consider that the 7.4-ps intersystem crossing of the S_1 state of $[Cu(dmphen)_2]^+$ is "extraordinarily" slow. This time constant might just indicate a wide range of intersystem crossing times of metal complexes, which can be significantly changed by the change in the spin−orbit coupling and the energy gap between the singlet and triplet states.[17] Our knowledge about ultrafast dynamics of metal

(52) It has been pointed out that the oscillator strength of the $S_1^{flattened}$ state can be larger than that of the S_1^{perp} state because the relevant transition is optically forbidden at the perpendicular structure (D_{2d}) but becomes optically allowed at the flattened structure (D_2) (ref 17). Therefore, in the quantitative sense, the ϕ_2 value may be somewhat less than unity. Nevertheless, the quantitative discussion based on the transition intensity is not straightforward, because the vibronic coupling between S_1 and S_2 states can also contribute to the intensity of $S_1 \leftarrow S_0$ transition significantly.

Table 1. Properties of Low-Lying Excited States of $[Cu(dmphen)_2]^+$ in Dichloromethane at Room Temperature

structure	emitting state	symmetry	λ^{max}/nm	lifetime/ps	radiative rate constant /10^6 s^{-1} (oscillator strength)[a]	
D_{2d}	S_2^{perp}	$^1B_2$	500	0.045	36[b] (0.13)	36[c] (0.135)
	S_1^{perp}	$^1A_2$	~600	0.66	1.8[b] (0.010)	3.0[c] (0.016)
D_2	$S_1^{flattened}$	$^1B_1$	720	7.4	1.6[b] (0.012)	2.2[d], 20[e]
	$T_1^{flattened}(+ S_1^{flattened})$[g]		770	4.1×10^4	0.0023[f]	

[a] Radiative rate constant (k_r) and oscillator strength (f) in parentheses are related with each other by an equation: $f = 1.50 \cdot k_r/\nu_{max}^2$. The k_r values were estimated by several methods: [b]present study, [c]absorption coefficient (ref 17), [d]emission quantum yield and lifetime (ref 17), [e]temperature dependence of steady-state emission spectrum (delayed fluorescence) (ref 45), and [f]apparent value estimated from the emission quantum yield and the lifetime using $k_r = \phi/\tau$ (ref 45). [g] This emission has a partial contribution of the delayed fluorescence of $S_1^{flattened}$ (ref 45).

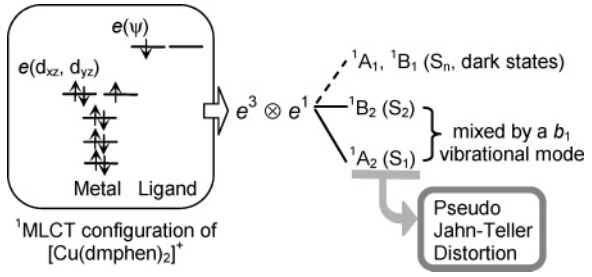

Figure 7. Electronic configuration of the ^{1}MLCT state of $[Cu(dmphen)_2]^+$. HOMO of $[Cu(dmphen)_2]^+$ is characterized by d_{xz} and d_{yz} orbital of metal center, and LUMO is characterized by ψ type orbital of the ligand. Because both are degenerated, the symmetry of ^{1}MLCT states is $E \otimes E = A_1 + A_2 + B_1 + B_2$.

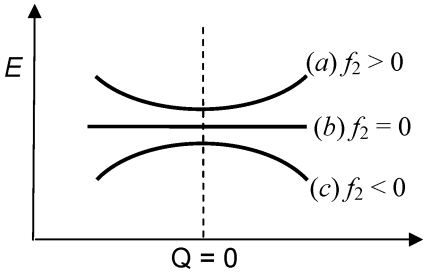

Figure 8. A sketch of the potential energy surface for the three cases of $f_2 > 0$, $f_2 = 0$, and $f_2 < 0$.

complexes is still limited, and more studies are necessary to have a common sense on the time scale of their ultrafast processes.

Excited-State Dynamics and a Realistic Potential Curve of "Pseudo Jahn–Teller" Distortion. The present time-resolved emission study provided unambiguous assignments of the excited-state dynamics and transients observed in the femto- and picosecond time region after photoexcitation of $[Cu(dmphen)_2]^+$. The dynamics of the ultrafast structural distortion ("flattening motion") was successfully distinguished from the other relaxation process, and it is now clear that it occurs in the S_1 state with a time constant of 660 fs in dichloromethane. On the basis of the results of experiments and analysis, we are now able to discuss the mechanism of the structural distortion that occurs on the S_1 potential surface of $[Cu(dmphen)_2]^+$.

The electronic configuration of the ^{1}MLCT excited state of $[Cu(dmphen)_2]^+$ is depicted in Figure 7. The d orbitals of the central copper are separated into four groups, i.e., degenerated d_{xz} and d_{yz}, and nondegenerated d_{xy}, $d_{x^2-y^2}$, and d_{z^2} in the order of energy, at the perpendicular D_{2d} geometry. Although all the orbitals are occupied in Cu(I) (d^{10}), MLCT excitation transfers one electron to the ligands, and the electronic state of the resultant Cu(II) (d^9) comes to have the degenerated E symmetry. (This is the reason some people considered the mechanism of structural distortion as the Jahn–Teller effect.[11,13,17]) From the ligand side, MLCT excitation transfers one electron to the LUMO that has E symmetry.[18,20,44] Therefore, from the viewpoint of the molecular orbital of the whole molecule, the ^{1}MLCT state(s) can have symmetries deduced from $E \otimes E$, which are $^1A_1$, $^1B_1$, $^1B_2$, and $^1A_2$. Among these four, only the $^1B_2$ state is optically allowed, and it has been assigned to the S_2 state that exhibits a strong absorption band peaked at 460 nm. The S_1 state is assigned to the optically forbidden $^1A_2$ state which appears in the absorption spectra with a small intensity.[17,44] Therefore, the ultrafast structural distortion of ^{1}MLCT state is the problem of the potential energy surface of the S_1 ($^1A_2$) state. This structural distortion has been considered as a pseudo Jahn–Teller effect in the literature.[20]

The Jahn–Teller distortion is discussed on the basis of the following expansion of the potential curve of the relevant electronic state with respect to a nuclear coordinate:[34–37]

$$E(Q) = E_1 + \left\langle \psi_1 \left| \frac{\partial \hat{H}}{\partial Q} \right| \psi_1 \right\rangle Q + \left(\frac{1}{2} \left\langle \psi_1 \left| \frac{\partial^2 \hat{H}}{\partial Q_i^2} \right| \psi_1 \right\rangle + \sum_{n \neq 1} \frac{\left| \left\langle \psi_n \left| \frac{\partial \hat{H}}{\partial Q} \right| \psi_1 \right\rangle \right|^2}{E_1 - E_n} \right) Q^2 \quad (5)$$

$$= E_1 + f_1 Q + f_2 Q^2 \quad (6)$$

where $\hat{H}$ and ψ_1 denote the Hamiltonian and wavefunction of the molecule. When the electronic state is degenerated, the second term (the f_1 factor) can have a nonzero value, at least for one nontotally symmetric coordinate Q, and hence gives a linear Q-dependence. It means that the potential curve has a finite slope at the unperturbed structure ($Q = 0$), and the structural distortion takes place along the Q coordinate, lowering the symmetry of the molecular structure. This is the (first-order) Jahn–Teller effect. In the case of the ^{1}MLCT state of $[Cu(dmphen)_2]^+$, this linear term vanishes for nontotally symmetric vibrations because the S_1^{perp} state has the nondegenerated $^1A_2$ symmetry. The structural stability in this case is discussed for the quadratic Q^2 terms, which determines the curvature of the potential curve at the $Q = 0$ geometry. The sign of the curvature is determined by the relative magnitude of the two terms in the quadratic Q^2 term. Among the two, the first term is positive, and the second term arising from the vibronic coupling is expected to be negative. If the balance of the two terms makes the f_2 value negative ($f_2 < 0$), the potential curve exhibits a parabolic feature opening downward (Figure 8c). This bears spontaneous structural instability and induces the structural distortion (pseudo Jahn–Teller effect or the second-order Jahn–

Teller effect).[35,36] On the other hand, it is considered that the structural distortion is not induced when the f_2 value is equal to or greater than zero ($f_2 \geq 0$), because a local minimum appears in the potential curve at the $Q = 0$ geometry (Figure 8a,b).

In the present study, it was revealed that the S_1^{perp} state is first generated on the S_1 potential and then undergoes the structural distortion to form the $S_1^{flattened}$ state with the time constant $\tau_2 = 660$ fs. As the time-resolved emission spectra show (Figure 4B), the corresponding temporal change of the fluorescence spectra clearly exhibits an isosbestic point at 675 nm. This means that the S_1^{perp} state exhibits an inherent fluorescence spectrum and that the temporal change of the time-resolved spectra can be understood by the decay of the S_1^{perp} fluorescence and the corresponding rise of the $S_1^{flattened}$ fluorescence. In other words, we did not observe any gradual red shift of the fluorescence spectra during the structural distortion, which is expected for the S_1 potential curve whose parabolic feature opens downward. It implies that the S_1^{perp} state (the precursor of the structural distortion) is a bound state in the local minimum on the S_1 potential and is separated from the $S_1^{flattened}$ state by a very small energy barrier on the potential energy surface. This situation is essentially different from the ordinary picture of the Jahn−Teller distortion, because the Jahn−Teller distortion is induced spontaneously by the instability of the molecule at the unperturbed structure. The present ultrafast emission study indicates that the S_1 potential energy surface of $[Cu(dmphen)_2]^+$ is rather flat but exhibits a parabolic feature opening a little upward at the perpendicular configuration ($Q = 0$), which makes the S_1^{perp} state a bound state and remain undistorted in the finite lifetime $\tau_2 = 660$ fs before the structural distortion. The excited-state structural dynamics of the Cu(I) complex cannot be determined simply by the potential feature at $Q = 0$, and in this sense, the mechanism of the structural distortion is more complicated than that expected by the simple discussion based on the Jahn−Teller theory. Theoretical calculations for the shape of the excited-state potential energy surface are desirable to obtain a more profound insight into the dynamics and mechanism of the structural distortion of the metal complexes.

We summarize the dynamics of the electronic relaxation and structural distortion of the $[Cu(dmphen)_2]^+$ complex in Figure 9, which has been revealed in the present study. With photoexcitation at 420 nm, the initially populated S_2^{perp} state emits strong fluorescence around 500 nm. It undergoes electronic relaxation with a time constant as short as 45 fs and is converted to the S_1^{perp} or T_1^{perp} state with a branching ratio of 7:3. The S_1^{perp} state shows a broad fluorescence spectrum extending from 550 to 750 nm. Although this S_1^{perp} state undergoes ultrafast structural change, its potential energy surface shows a parabolic form opening a little upward, at least, at the unperturbed structure. Accordingly, the S_1^{perp} state stays undistorted, as long

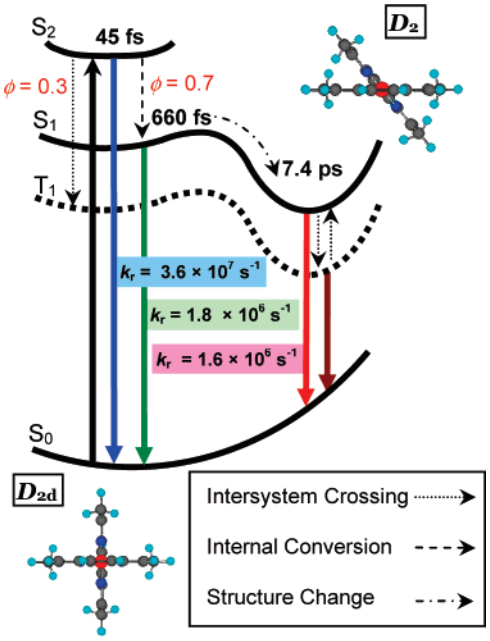

Figure 9. Scheme of the electronic relaxation and structural distortion of $[Cu(dmphen)_2]^+$ in dichloromethane after S_2 excitation.

as 660 fs. The structural distortion of the $[Cu(dmphen)_2]^+$ complex takes place with this 660-fs time constant, giving rise to the $S_1^{flattened}$ state having a distorted structure (D_2 symmetry). The change of the fluorescence spectrum in the course of this structural distortion clearly shows an isoemissive point, indicating that there is a very small but finite potential barrier between the S_1^{perp} and $S_1^{flattened}$ states. The $S_1^{flattened}$ state emits fluorescence around 720 nm, and it undergoes the intersystem crossing to the $T_1^{flattened}$ state with the 7.4-ps time constant. The T_1^{perp} state, which is formed by the direct intersystem crossing from the S_2^{perp} state, is also converted to the same $T_1^{flattened}$ state by the structural distortion in the triplet manifold. The $T_1^{flattened}$ state emits phosphorescence with the 41-ns lifetime in the 700−800 nm region, which is predominant in the steady-state emission spectrum.

Acknowledgment. We acknowledge sincere comments from Prof. E. W. Castner, Jr. While we were preparing this manuscript, we heard from him that they observed essentially the same time-resolved emission data in their up-conversion experiments that were undertaken independently.

Supporting Information Available: Full data of ultrafast emission time profile obtained by the up-conversion method and details of the analysis for femtosecond and picosecond time-resolved emission data.

JA069300S